Ultrafast Photoinduced Electric-Polarization Switching in a Hydrogen-Bonded Ferroelectric Crystal

K. Iwano,[1] Y. Shimoi,[2] T. Miyamoto,[3] D. Hata,[3] M. Sotome,[3] N. Kida,[3] S. Horiuchi,[4] and H. Okamoto[3,5]
[1]*Graduate University for Advanced Studies, Institute of Materials Structure Science, High Energy Accelerator Research Organization (KEK), Tsukuba 305-0801, Japan*
[2]*Research Center for Computational Design of Advanced Functional Materials, National Institute of Advanced Industrial Science and Technology (AIST), Tsukuba 305-8568, Japan*
[3]*Department of Advanced Materials Science, University of Tokyo, Chiba 277-8561, Japan*
[4]*Flexible Electronics Research Center, National Institute of Advanced Industrial Science and Technology (AIST), Tsukuba 305-8565, Japan*
[5]*AIST-UTokyo Advanced Operando-Measurement Technology Open Innovation Laboratory (OPERANDO-OIL), National Institute of Advanced Industrial Science and Technology (AIST), Chiba 277-8568, Japan*
(Received 24 November 2016; published 10 March 2017)

Croconic acid crystals show proton displacive-type ferroelectricity with a large spontaneous polarization reaching 20 $\mu C/cm^2$, which originates from the strong coupling of proton and π-electron degrees of freedom. Such a coupling makes us expect a large polarization change by photoirradiations. Optical-pump second-harmonic-generation-probe experiments reveal that a photoexcited croconic-acid crystal loses the ferroelectricity substantially with a maximum quantum efficiency of more than 30 molecules per one absorbed photon. Based on density functional calculations, we theoretically discuss possible pathways toward the formation of a one-dimensional domain with polarization inversion and its recovery process to the ground state by referring to the dynamics of experimentally obtained polarization changes.

DOI: 10.1103/PhysRevLett.118.107404

The physics of photoinduced phase transitions (PIPTs) has recently been attracting significant attention [1,2]. The basic strategy for its understanding is to recognize hidden associations between the electronic excitations provided by light and other degrees of freedom in matter. Among them, the most direct association is considered to be the electronic PIPTs, which are observed, for example, in the ultrafast metallizations of Mott insulators [3–11]. In this case, the initial local electronic excitation immediately changes the surrounding electron systems via electron-electron interactions, leading to global electronic phase changes occurring on time scales of 1–10 fs. In contrast, when atomic motions are induced by electronic excitations in the PIPTs, the association is less direct [12–16], and the time scales are inevitably slower because of the photoconversions of both electronic and atomic states [17]. Depending on the systems, the time scale varies from sub-ps to several 10 ps, of which the orders would be determined by vibrational periods along the reaction path of the PIPTs.

Here, we propose another type of association via electron-proton interaction: an electronic π-π^* excitation in an organic molecule induces the movements of the surrounding protons. In Fig. 1(a), we show a part of the croconic-acid crystal, which is known to exhibit ferroelectricity with large polarization reaching 20 $\mu C/cm^2$ [18]. Its polarization is directed along the c axis, being within its layered structure. As depicted there, the proton moves along the c axis leading to the polarization change, which suggests a proton displacive-type ferroelectricity. It is remarkable that this ferroelectricity persists up to its decomposing temperature at 450 K and up to 5.3 GPa as a pressure [19]. In our previous study, we analyzed the optical reflectivity spectra and the excitation photon-energy dependence of the second harmonic generation (SHG), and suggested that the lowest π-π^* transition at around 3.2 eV [see Fig. 1(b)] is responsible for the SHG. We also calculated the molecular orbitals (MOs) relevant to the π-π^* transitions by means of a density-functional theory (DFT). The results indicated that the ground state has the MO weighted on the side to which the protons are attached, whereas the final state of the lowest π-π^* transition has the MO weighted on the other side [Fig. 1(c)] [20]. This means that the direction of the dipole moment in the lowest photoexcited state is opposite to that in the ground state.

In the complex nonlinear optical materials, it is important to distinguish a functional building unit responsible for SHG or equivalently an optically active center and clarify its nature [21–23]. The unique feature of the croconic acid crystal is that the π-electron system in each molecule, which is the optically active center of this material, interacts with π-electron systems of the neighboring molecules through hydrogen bonds. Considering this feature, we expect that the reversal of the dipole moment in the photoexcited state would make the surrounding protons unstable, giving rise to their displacements. As a result, a finite spatial size of domain in which the polarization is inverted with proton displacements would be generated. To investigate such a photoinduced phenomenon, in the

 © 2017 American Physical Society

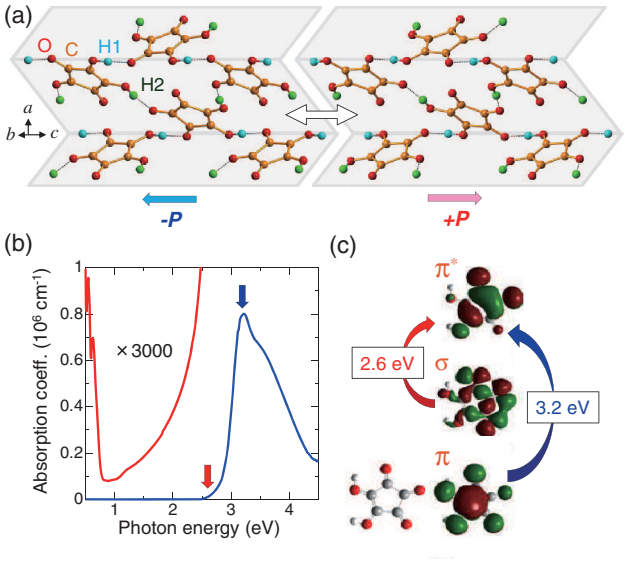

FIG. 1. (a) Crystal structures of croconic acid with opposite directions of ferroelectric polarization P. (b) The optical absorption spectrum along the c axis. Arrows show pump photon energies in the pump-probe experiments. (c) Molecular orbitals of an isolated croconic-acid molecule. Pump photon energies of 3.2 and 2.6 eV correspond to the lowest π-π^* transition and the σ-π^* transition, respectively.

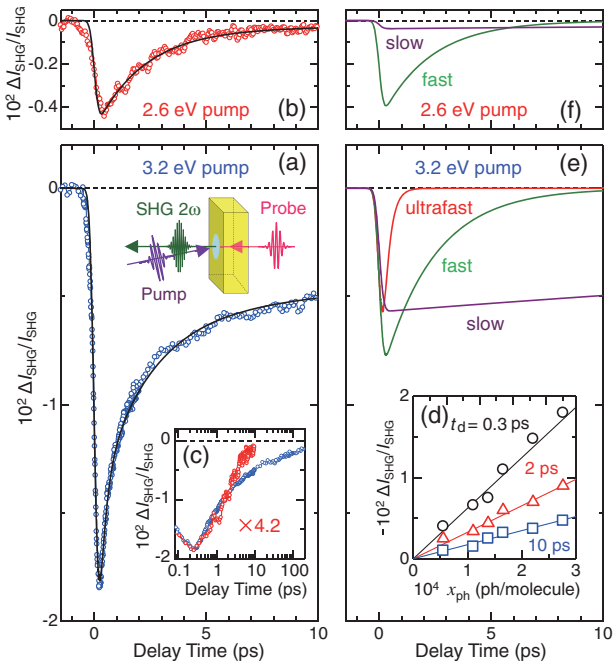

FIG. 2. (a, b) Time evolutions of $\Delta I_{\mathrm{SHG}}/I_{\mathrm{SHG}}$ by the pump light with (a) 3.2 eV and $x_{\mathrm{ph}} = 2.8 \times 10^{-4}$ ph/molecule and (b) 2.6 eV and $x_{\mathrm{ph}} = 1.5 \times 10^{-4}$ ph/molecule (open circles). Solid lines show fitting curves. The experimental configuration is illustrated in the inset of Fig. 2(a). (c) Semilogarithmic plots of time evolutions shown in (a) and (b). (d) x_{ph} dependence of $\Delta I_{\mathrm{SHG}}/I_{\mathrm{SHG}}$ at several typical delay times. (e),(f) Each component of fitting curves shown in (a) and (b) (see the text).

present study, we perform optical-pump SHG-probe measurements in croconic acid crystals and analyze the results theoretically.

In the past, analogous materials were discussed from the viewpoint of proton dynamics. For example, pressure effects were studied for several hydrogen-bonded molecular chains and the formation of kink solitons associated with hydrogen bonds under pressure was claimed [24]. Very recently, a hydrogen-bonded ferroelectric system consisting of protonated 2,3-di(2-pyridinyl)pyrazine (H-dppz) and deprotonated chlor-anilic acid (Hca) was reported to show photoinduced suppression of the SHG intensity [25], although no detailed theoretical mechanism was unraveled.

Single crystals of croconic acid were grown by a previously reported method [18,26]. To investigate photoinduced polarization changes, we used transmission-type SHG as a probe, since its intensity (I_{SHG}) depends on the polarization amplitude. The photon energies of the incident and SH lights were 0.95 and 1.9 eV, respectively. The photon energy of the pump light was set at 3.2 and 2.6 eV, which correspond to the lowest π-π^* transition [20] and the σ-π^* transition [20,27], respectively. The pump and probe lights were obtained by two optical parametric amplifiers, which were excited by an output of the Ti:sapphire regenerative amplifier (repetition rate: 1 kHz, photon energy: 1.58 eV, and pulse width: 130 fs). The experimental setup is schematically shown in the inset of Fig. 2(a). According to the THz-radiation imaging experiment [28], the ferroelectric domain was uniform in the depth direction, i.e., the b axis, and its size was larger than the spot diameters of the pump and probe pulses. Since the SH light was generated only from the back part of the crystal because of the short coherence length l_C ($= 1.4\ \mu$m) [20], the pump light was incident from the back side. The time resolution was 0.37 ps. The excitation photon density (x_{ph}) is defined as an averaged value in the back part with the thickness of the coherence length, which is expressed by $x_{\mathrm{ph}} = (1 - R_{\mathrm{ex}})[1 - \exp(-l_C/l_{\mathrm{ex}})]I_{\mathrm{ex}}/l_C$. Here, R_{ex}, l_{ex}, and I_{ex} are the reflectivity, the penetration length, and the photon density per unit area of the pump light, respectively. All the experiments were performed at 294 K in vacuum.

Figures 2(a), [2(b)], and 2(c) show the photoinduced decrease of the SHG intensities $\Delta I_{\mathrm{SHG}}/I_{\mathrm{SHG}}$ by the pump light with 3.2 eV and $x_{\mathrm{ph}} = 2.8 \times 10^{-4}$ photons(ph)/molecule (with 2.6 eV and $x_{\mathrm{ph}} = 1.5 \times 10^{-4}$ ph/molecule). The decrease of the SHG within the time resolution is attributable to the decrease of the ferroelectric polarization via the changes in the π electron wave functions and the proton configurations. $(-\Delta I_{\mathrm{SHG}}/I_{\mathrm{SHG}})$ for the 3.2 eV excitation increases linearly with x_{ph} at 0.3, 2, and 10 ps in common, indicating that the relaxation dynamics of

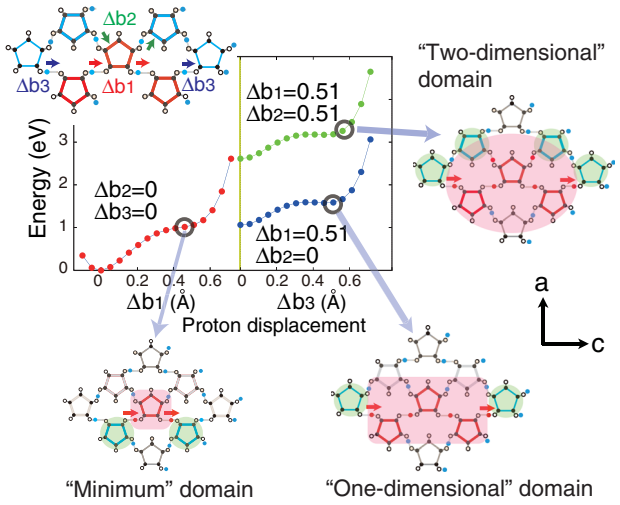

FIG. 3. Adiabatic potential curves in the electronic ground state and schematic illustrations corresponding to the configurations. The carbon rings in the inner part of the domain and those within the DWs are shaded by pink and green colors, respectively.

the photoexcited state does not change with x_{ph} [Fig. 2(d)]. To discuss the observed change of the SHG, we assume that a certain number of molecules completely lose their dipole moments and that the second-order nonlinear susceptibility is proportional to the polarization magnitude P ($I_{\mathrm{SHG}} \propto P^2$) and, thus $\Delta I_{\mathrm{SHG}}/I_{\mathrm{SHG}} \sim 2\Delta P/P$. On the basis of these assumptions, we define the efficiency for the polarization decrease as the number of those molecules per photon, which is evaluated to be ~32 (~14) molecules/ph at 3.2 eV (2.6 eV) pump. To evaluate the relaxation time of the change in the SHG intensity, we performed fitting analyses by using the following formula, which is convolved with a Gaussian function with a width of 0.37 ps (the time resolution):

$$\frac{\Delta I_{\mathrm{SHG}}}{I_{\mathrm{SHG}}} = -\sum_i A_i \exp(-t/\tau_i) \quad (i = 1-3). \qquad (1)$$

Here, τ_1 (A_1), τ_2 (A_2), and τ_3 (A_3) are the relaxation times (the amplitudes) for the ultrafast, fast, and slow decay components, respectively [29]. The experimental results can be well reproduced by the fitting curves [black lines in Figs. 2(a), 2(b)]. Three components ($i = 1$, 2, and 3) are also shown by red, green, and purple lines, respectively, in Figs. 2(e) and 2(f). The obtained relaxation times are $\tau_1 = 0.27$, $\tau_2 = 2.2$, and $\tau_3 \gg 10$ ps for the 3.2 eV excitation and $\tau_2 = 2.3$ and $\tau_3 \gg 10$ ps for the 2.6 eV excitation. Note that the ultrafast decay component appears only for the 3.2 eV excitation and that the slow decay component for the 3.2 eV excitation is much larger than that for the 2.6 eV excitation [Fig. 2(c)].

To interpret the above experimental results, we applied DFT [30] to molecular clusters, including excited state calculations based on time-dependent DFT [31]. Because the details of the method are described in the Supplemental Material [32], we here mention only the results. First, we calculated adiabatic potential curves for several conditions. In Fig. 3, we summarize the results for the electronic ground states of a cluster consisting of nine molecules. Here, we use three displacements of hydrogen atoms along each bond, Δb_1, Δb_2, and Δb_3, which are specified in the illustrations at the upper left of Fig. 3. First of all, we discuss the movements represented by Δb_1. We simultaneously move the two hydrogen atoms attached to the central molecule. Because the initial O-H distances for the short and long pairs are 1.02 and 1.58 Å, respectively, a displacement around 0.5 Å almost exchanges the long and short bonds. In fact, we find a slight minimum around $\Delta b_1 = 0.51$ Å in the conditions of $\Delta b_2 = 0$ and $\Delta b_3 = 0$ (red curve). As illustrated in the lower-left part in Fig. 3, this state is regarded as a "minimum domain" or a pair of domain walls (DWs) with one inner molecule (shaded area).

We next pay attention to extensions of this domain. A possible extension is that for the "one-dimensional domain," of which the potential energy is plotted by the blue curve as a function of Δb_3, with $\Delta b_1 = 0.51$ Å and again $\Delta b_2 = 0$. We regard this as a domain consisting of two DWs and three inner molecules (shaded area in the lower-right cartoon). We also calculated the case of a "two-dimensional" domain as plotted by the green curve. Here, the upper hydrogen atoms are already moved to another metastable state, namely, of $\Delta b_2 = 0.51$ Å, and the potential energy is plotted as a function of Δb_3. As is seen clearly, this case needs a much larger energy to form a domain. We relate this energy increase to the number of molecules forming the DWs. In fact, the number of molecules is four in this case, whereas those in the previous two cases are two. This energy increase for the molecules in the DWs is interpreted as being caused by the nature of a charged DW [35]. Namely, the molecules in the DWs have one or three hydrogen atoms, whereas the number of electrons in those molecules does not change from the original value. Because the hydrogens have positive valencies, the molecules are therefore charged positively or negatively, causing extra Coulombic energies. Comparing the two types of extensions, the one-dimensional extension seems to be more easily realized. Such tendency is also found in the microscope images of ferroelectric domains in the croconic acid crystal [28] and other materials [35,36], as a prevalence of one-dimensional domains, that are, line- or stripe-type domains running along the polarization direction.

We also estimate a maximum domain size for the case of the one-dimensional domain as follows. The formation energy for a domain consisting of n molecules, $E_{\mathrm{form}}(n)$, is formulated approximately as $E_{\mathrm{form}}(n) = E_{\mathrm{DW}} + n\Delta_{\mathrm{int}}$, where E_{DW} is the DW pair energy and Δ_{int} the internal energy per one molecule. For example, the minimum domain and the one-dimensional domain in Fig. 3 correspond to $n = 1$ and $n = 3$, respectively. We then use their energies at $(\Delta b_1, \Delta b_3) = (0.51, 0)$ and (0.51, 0.51) with $\Delta b_2 = 0$

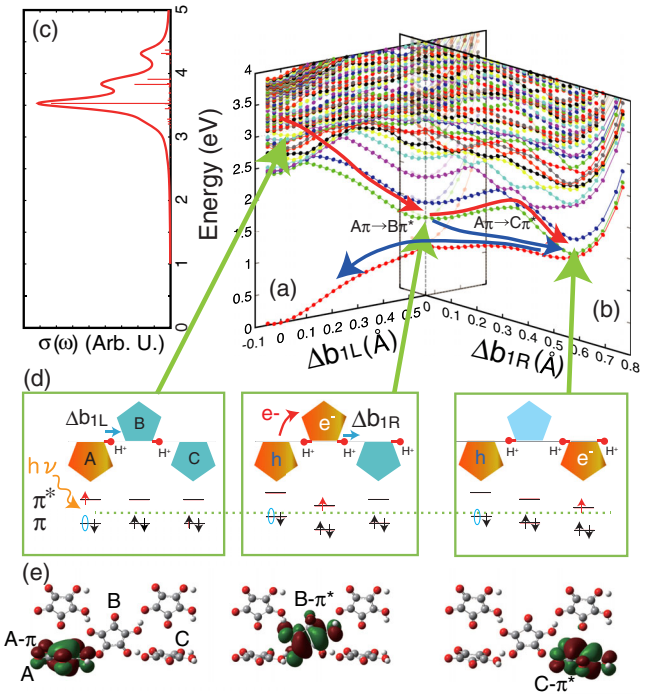

FIG. 4. (a) and (b) Adiabatic potential curves corresponding to the electronic ground and excited states, (c) optical conductivity spectrum, (d) schematics for the electron transitions, and (e) associated molecular orbitals. In (b), Δb_{1L} is fixed at 0.55 Å. The arrow drawn from the rightmost panel in (d) points the first excited state in (b).

commonly, as $E(1)$ and $E(3)$, respectively. E_{DW} and Δ_{int} are, consequently, evaluated to be 0.75 and 0.25 eV, respectively. By a further analysis assuming an asymmetric deformation of the carbon ring, we find a smaller Δ_{int} of 0.20 eV, as shown in the Supplemental Material [32]. Using the excitation energy of 3.2 eV and making it equal to $E_{\mathrm{form}}(n)$, we obtain $n \sim 12$. As is explained in the Supplemental Material [32], this number corresponds to the effective polarization reversal of 10 molecules by one photon. We note that the experimental estimation of photoinduced ferroelectricity disappearance (32 molecules for a 3.2 eV pump, for example) is obtained by assuming zero polarizations in a domain. The theoretical evaluation of 10 for the molecules with polarization reversals is comparable to the case that 20 molecules lose their polarization, being comparable to the experimental number.

In order to discover a possible pathway for the domain growth after the photoexcitation, we investigated the excited states of a five-molecule cluster. In Figs. 4(a) and 4(b), we show adiabatic potential energy curves up to 4 eV, together with the corresponding optical conductivity spectrum for the light polarization parallel to the c axis in Fig. 4(c). First, we discuss the energy curves in Fig. 4(a), as a function of Δb_{1L}. Here, we distinguish the two displacements of Δb_1 and name the left and right ones Δb_{1L} and Δb_{1R}, respectively. The origin in Fig. 4(a) corresponds to the structure with all the displacements being zero, and only Δb_{1L} was changed there. The spectrum was obtained for the structure at this origin. We first notice the presence of several low-lying excited states below the absorption peak. They are intramolecular σ-π^* excitations and considered to be the main component of the low-energy tail seen in Fig. 1(b) (red curve). Furthermore, we find a rather large energy relaxation for some of the lowest excited states. In particular, the amount of energy relaxation from the initial photoexcited state along the lowest excited state [red arrow in Fig. 4(a)] is around 2.3 eV. This relaxation reduces the excited state energy to about 1.2 eV at $\Delta b_{1L} = 0.55$ Å, being comparable to the energy of the potential curve for the ground state. We attribute this relaxation to the change in the relative potential energies at the associated molecules. Namely, as shown in the left panel of Fig. 4(d), the initial π to π^* excitation within the molecule A prompts one of its nearby hydrogens to move to the right, due to generated charge unbalance in the excited state. We then expect the elevation (lowering) of the energy levels of the molecule A (B) as shown in the middle panel, because the hydrogen is positively charged with the valency of ~0.5. These elevation and lowering consequently cause the electron-transferred state, namely, an electron in the B-π^* orbital and a hole in the A-π orbital [see MOs in Fig. 4(e)], to relax to the lower energy as already mentioned.

We finally discuss the behavior of a further relaxation represented by another displacement, Δb_{1R}, fixing the value of Δb_{1L} at 0.55 Å. As illustrated by the right panel in Fig. 4(d), this hydrogen movement changes the potentials at the molecules B and C and, finally, at the end point near C, the site energy at A (C) is the highest (lowest). This rearrangement induces further electronic relaxation in the excited state [red arrow in Fig. 4(b)], that is, the electron and the hole in the C-π^* orbital [rightmost MO in Fig. 4(e)] and the A-π orbital, respectively. Another important pathway is along the blue rightwards arrow in Fig. 4(b). In this case, an electron-hole pair recombines at around $(\Delta b_{1L}, \Delta b_{1R}) = (0.55, 0)$ and a subsequent proton transfer occurs from the B molecule to the C molecule. This process will be possible using the excess energy originating from the electron-hole recombination.

On the basis of the theoretical analyses presented above, we discuss the origin of the three components experimentally observed in Fig. 2. First, the slow decay component is attributable to the relaxation process of the state shown in the right panel of Fig. 4(d) and other similar states in which the two DWs are more spatially separated. The presence of a finite amount of energy barrier delays the relaxations of those states. Namely, the states are metastable. To reach these metastable states, large excess energy will be necessary, and this is the reason why the slow decay component reflecting the metastable states is large for the 3.2 eV excitation as compared to the case for the 2.6 eV excitation. Second, the fast delay component is assigned to the structural relaxation from the "one-dimensional" domain (the right-lower panel in Fig. 3 or

other similar configurations) within the electronic ground state. Note that no electron-hole separation occurs for such states. They are directly connected to the initial homogeneously ferroelectric state on the ground-state potential surface [the blue leftwards arrow in Figs. 4(a) and 4(b)], so that the decay is fast. Regarding the ultrafast decay component, it is observed only for the 3.2 eV excitation. As a general tendency, we expect that high energy excitations will yield states in that the electron and proton degrees of freedom are correlated quantum-mechanically and, hence, can reasonably attribute such states to the ultrafast component, although they are not treated in the present theoretical analyses.

In conclusion, we observed the photoinduced decease of ferroelectric polarization in croconic acid crystals. The DFT calculation revealed that an effective pathway of the polarization reversal in a semimacroscopic region really exists. This study will deepen the understanding on photoinduced proton-electron-coupled dynamics, and lead to further explorations of novel optical phenomena in hydrogen-bonded molecular ferroelectrics. Moreover, the photoinduced polarization reversal and its rapid recovery as reported here will be able to be used in new optical devices, in which optical responses can be modulated or switched by optical pulses in the picosecond time scale.

This study was supported by the Grant-In-Aid (KAKENHI: No. 25400334) from the Ministry of Education, Science, Culture, and Sports of Japan, and CREST, Japan Science and Technology Agency.

[1] *Relaxations of Excited States and Photoinduced Structural Phase Transitions*, Springer Series in Solid State Science, edited by K. Nasu (Springer-Verlag, Berlin, 1997), Vol. 124.
[2] K. Yonemitsu and K. Nasu, Phys. Rep. **465**, 1 (2008).
[3] S. Iwai, M. Ono, A. Maeda, H. Matsuzaki, H. Kishida, H. Okamoto, and Y. Tokura, Phys. Rev. Lett. **91**, 057401 (2003).
[4] H. Okamoto, H. Matsuzaki, T. Wakabayashi, Y. Takahashi, and T. Hasegawa, Phys. Rev. Lett. **98**, 037401 (2007).
[5] H. Okamoto, T. Miyagoe, K. Kobayashi, H. Uemura, H. Nishioka, H. Matsuzaki, A. Sawa, and Y. Tokura, Phys. Rev. B **82**, 060513(R) (2010).
[6] F. Novelli, G. De Filippis, V. Cataudella, M. Esposito, I. Vergara, F. Cilento, E. Sindici, A. Amaricci, C. Giannetti, D. Prabhakaran, S. Wall, A. Perucchi, S. D. Conte, G. Cerullo, M. Capone, A. Mishchenko, M. Grüninger, N. Nagaosa, F. Parmigiani1, and D. Fausti, Nat. Commun. **5**, 5112 (2014).
[7] M. Eckstein and P. Werner, Sci. Rep. **6**, 21235 (2016).
[8] Z. LenarčIč and P. Prelovšek, Phys. Rev. Lett. **111**, 016401 (2013).
[9] E. Iyoda and S. Ishihara, Phys. Rev. B **89**, 125126 (2014).
[10] D. Golež, J. Bonča, M. Mierzejewski, and L. Vidmar, Phys. Rev. B **89**, 165118 (2014).
[11] M. Segawa, A. Takahashi, H. Gomi, and M. Aihara, J. Phys. Soc. Jpn. **80**, 084721 (2011).
[12] Y. Toyozawa, Physica (Amsterdam) **117–118B**, 23 (1983).
[13] E. Hanamura and N. Nagaosa, J. Phys. Soc. Jpn. **56**, 2080 (1987).
[14] Y. Toyozawa, Solid State Commun. **84**, 255 (1992).
[15] S. Koshihara and S. Adachi, J. Phys. Soc. Jpn. **75**, 011005 (2006), and references therein.
[16] M. Gao, C. Lu, H. Jean-Ruel, L. Liu, A. Marx, K. Onda, S. Koshihara, Y. Nakano, X. Shao, T. Hiramatsu, G. Saito, H. Yamochi, R. Cooney, G. Moriena, G. Sciaini, and R. Dwayne Miller, Nature (London) **496**, 343 (2013).
[17] A. Cavalleri, T. Dekorsy, H. H. W. Chong, J. C. Kieffer, and R. W. Schoenlein, Phys. Rev. B **70**, 161102(R) (2004).
[18] S. Horiuchi, Y. Tokunaga, G. Giovanetti, S. Picozzi, H. Itoh, R. Shimano, R. Kumai, and Y. Tokura, Nature (London) **463**, 789 (2010).
[19] M. Sikora, P. Pojawis, and A. Katrusiak, J. Phys. Chem. C **117**, 14213 (2013).
[20] R. Sawada, H. Uemura, M. Sotome, H. Yada, N. Kida, Y. Shimoi, S. Horiuchi, and H. Okamoto, Appl. Phys. Lett. **102**, 162901 (2013).
[21] A. Cammarata, W. Zhang, P. S. Halasyamani, and J. Rondinelli, Chem. Mater. **26**, 5773 (2014).
[22] A. Cammarata and J. M. Rondinelli, ACS Photonics **1**, 96 (2014).
[23] A. Cammarata and J. Rondinelli, J. Mater. Chem. C **4**, 5858 (2016).
[24] Y. Moritomo, Y. Tokura, T. Oonishi, T. Kojima, and A. Itsubo, J. Chem. Phys. **96**, 8507 (1992).
[25] T. Umanodan, S. Tanaka, S. Naruse, T. Ishikawa, K. Onda, S. Koshihara, S. Horiuchi, and Y. Okimoto, J. Phys. Soc. Jpn. **84**, 073707 (2015).
[26] D. Braga, L. Maini, and F. Grepioni, CrystEngComm **3**, 27 (2001).
[27] C. Ramachandran and E. Ruckenstein, Comput. Theor. Chem. **973**, 28 (2011).
[28] M. Sotome, N. Kida, S. Horiuchi, and H. Okamoto, Appl. Phys. Lett. **105**, 041101 (2014).
[29] The $\Delta I_{\mathrm{SHG}}/I_{\mathrm{SHG}}$ signal for the 2.6-eV excitation is almost reproduced by a single exponential decay component (the fast decay component) [Figs. 2(b) and (f)]. In contrast, to reproduce the $\Delta I_{\mathrm{SHG}}/I_{\mathrm{SHG}}$ signal for the 3.2-eV excitation, the other two components (the ultrafast and slow decay components) are necessary in addition to the fast decay component [Figs. 2(a) and (e)].
[30] M. J. Frisch *et al.*, Gaussian 09, Revision B.01, Gaussian Inc., Wallingford, CT, 2010.
[31] R. E. Stratmann, G. E. Scuseria, and M. J. Frisch, J. Chem. Phys. **109**, 8218 (1998).
[32] See Supplemental Material at http://link.aps.org/supplemental/10.1103/PhysRevLett.118.107404 for calculation details, which includes Refs. [33,34].
[33] D. D. Sante, A. Stroppa, and S. Picozzi, Phys. Chem. Chem. Phys. **14**, 14673 (2012).
[34] R. Dovesi, R. Orlando, B. Civalleri, C. Roetti, V. R. Saunders, and C. M. Zicovich-Wilson, Z. Kristallogr. **220**, 571 (2005).
[35] F. Kagawa, S. Horiuchi, N. Minami, S. Ishibashi, K. Kobayashi, R. Kumai, Y. Murakami, and Y. Tokura, Nano Lett. **14**, 239 (2014).
[36] M. Sotome, N. Kida, S. Horiuchi, and H. Okamoto, ACS Photonics **2**, 1373 (2015).